AMERICAN SOCIETY FOR MICROBIOLOGY | mBio

Check for updates

| Virology | Research Article

Guanylate-binding protein 5 antagonizes viral glycoproteins independently of furin processing

Hana Veler,[1] Cheng Man Lun,[1] Abdul A. Waheed,[1] Eric O. Freed[1]

AUTHOR AFFILIATION See affiliation list on p. 18.

ABSTRACT Guanylate-binding protein (GBP) 5 is an interferon-inducible cellular factor with broad anti-viral activity. Recently, GBP5 has been shown to antagonize the glycoproteins of a number of enveloped viruses, in part by disrupting the host enzyme furin. Here we show that GBP5 strongly impairs the infectivity of virus particles bearing not only viral glycoproteins that depend on furin cleavage for infectivity—the envelope (Env) glycoproteins of HIV-1 and murine leukemia virus and the spike (S) glycoprotein of severe acute respiratory syndrome coronavirus 2 (SARS-CoV-2)—but also viral glycoproteins that do not depend on furin cleavage: vesicular stomatitis virus glycoprotein and SARS-CoV S. We observe that GBP5 disrupts proper *N*-linked protein glycosylation and reduces the incorporation of viral glycoproteins into virus particles. The glycosylation of the cellular protein CD4 is also altered by GBP5 expression. Flow cytometry analysis shows that GBP5 expression reduces the cell-surface levels of HIV-1 Env and the S glycoproteins of SARS-CoV and SARS-CoV-2. Our data demonstrate that, under the experimental conditions used, inhibition of furin-mediated glycoprotein cleavage is not the primary anti-viral mechanism of action of GBP5. Rather, the antagonism appears to be related to impaired trafficking of glycoproteins to the plasma membrane. These results provide novel insights into the broad antagonism of viral glycoprotein function by the cellular host innate immune response.

IMPORTANCE The surface of enveloped viruses contains viral envelope glycoproteins, an important structural component facilitating virus attachment and entry while also acting as targets for the host adaptive immune system. In this study, we show that expression of GBP5 in virus-producer cells alters the glycosylation, cell-surface expression, and virion incorporation of viral glycoproteins across several virus families. This research provides novel insights into the broad impact of the host cell anti-viral factor GBP5 on protein glycosylation and trafficking.

KEYWORDS GBP5, viral glycoproteins, HIV-1 Env, MLV Env, SARS-CoV-2 S, SARS-CoV S, VSV-G, cellular inhibitory factors

The virions of many RNA viruses contain a lipid envelope in which viral glycoproteins that catalyze the fusion between the viral envelope and target cell membranes are embedded during virus entry. Three structural classes of viral fusion proteins have been described: classes I, II, and III (1). Examples of class I viral fusion proteins include the hemagglutinin (HA) protein of influenza A viruses (IAVs), the Env glycoproteins of retroviruses [e.g., gp120/gp41 of HIV-1 and gp70/p15(E) of murine leukemia virus (MLV)], the spike (S) proteins of coronaviruses (e.g., severe acute respiratory syndrome coronaviruses SARS-CoV and SARS-CoV-2), and the Ebola virus (EBOV) glycoprotein. class II fusion proteins include those of the flaviviruses, alphaviruses, and bunyaviruses. The prototype class III fusion protein is the glycoprotein of the rhabdovirus vesicular stomatitis virus glycoprotein (VSV-G). Class I fusion proteins form trimers that adopt highly stable,

Editor Stephen P. Goff, Columbia University Medical Center, New York, New York, USA

Address correspondence to Eric O. Freed, efreed@nih.gov.

The authors declare no conflict of interest.

See the funding table on p. 18.

Received 11 July 2024
Accepted 29 July 2024
Published 30 August 2024

rod-like structures with central trimeric α-helical coiled coils in the pre-fusion state, which refold into six-α-helical bundles in the post-fusion state (2, 3). They are synthesized as fusion-inactive precursors in the endoplasmic reticulum (ER), where they are modified by glycosylation (4). *N*-Linked glycosylation is initiated in the ER via *en bloc* transfer of a high-mannose oligosaccharide precursor to an Asn residue in an Asn-X-Ser/Thr motif (5). Properly folded precursor trimers then move to the *cis*-Golgi apparatus before being transferred to the medial-Golgi for maturation and exit via the *trans*-Golgi network (TGN). During trafficking through the Golgi, high-mannose oligosaccharide side chains can be modified to higher-molecular-weight, complex forms. Many viral glycoproteins undergo proteolytic cleavage by the cellular convertase furin or other furin-like enzymes during trafficking through the Golgi apparatus to produce two subunits: the receptor-binding subunit and the transmembrane subunit responsible for membrane fusion (6).

Pathogen invasion triggers the production of interferons (IFNs), leading to upregulated expression of IFN-stimulated genes (ISGs) that play important roles in the innate immune response. A subset of ISGs targets the function of viral glycoproteins (for review, see reference 7); these ISGs include certain guanylate-binding proteins (GBPs) such as GBP2 and GBP5. GBPs are members of the IFN-inducible GTPases that are among the most highly IFN-γ-induced genes (8, 9) and which contribute to the cell's innate immune defense against bacteria, protozoa, and viruses. For example, GBP1, the most well-studied member of the GBP family, restricts VSV (10), dengue viruses (11), encephalomyocarditis virus (a non-enveloped virus) (10), and hepatitis C virus (12, 13). GBP5 has been shown to act as an activator of NLRP3 inflammasome assembly and to play a role in innate immunity and inflammation (9). Early studies reported that GBP5 targets the viral envelope glycoproteins of IAV (14) and EBOV (15).

A genome-wide screen identified GBP5 as a potential HIV-1 restriction factor (16). Subsequently, it was demonstrated that GBP5 disrupts HIV-1 infectivity by targeting Env processing and virion incorporation (17). Significantly, the infectivity of HIV-1 particles produced from IFN-stimulated monocytic cells correlated inversely with the levels of GBP5 expression, suggesting that IFN-induced endogenous levels of GBP5 in a physiologically relevant cell type suppress HIV-1 infectivity (17). Further studies have shown that GBP5 and the related protein GBP2 disrupt HIV-1 infectivity by interfering with furin activity. Consistent with this result, the infectivity of virus particles bearing other viral glycoproteins that depend on furin cleavage for infectivity from rabies virus, European bat lyssa virus, Marburg virus, IAV, and MLV was inhibited by GBP2 and GBP5 expression (18). GBP5 was also found to reduce the infectivity of particles bearing the Lassa virus glycoprotein, which is activated not by furin but by the protease PCSK8 (18). A recent study reported that GBP2 and GBP5 inhibit the activity of the SARS-CoV-2 S glycoprotein, which depends on furin cleavage for infectivity (19). While these data suggest that GBP5 exerts its broad anti-viral activity by targeting cellular furin, the precise mechanism by which GBP5 inhibits processing of viral glycoproteins and whether it only affects protease-dependent viral glycoproteins remain poorly understood.

To understand the anti-viral mechanism of action of GBP5, we measured the effect of producer-cell GBP5 expression on the infectivity of virus particles bearing glycoproteins that depend on furin cleavage for infectivity and furin-independent glycoproteins from five different viruses: HIV-1, MLV, SARS-CoV, SARS-CoV-2, and VSV. GBP5 expression at physiological levels was found to reduce the infectivity of particles bearing the glycoproteins from each of these viruses and to cause a shift in the electrophoretic mobility of the viral glycoproteins as a result of altered *N*-linked glycosylation and/or glycan modification. Flow cytometry analysis indicated that GBP5 expression significantly reduces the cell-surface expression of HIV-1 Env, SARS-CoV S, and SARS-CoV-2 S. Our findings demonstrate that GBP5 antagonizes viral glycoproteins, including representatives of both class I and III fusion proteins, by impeding their trafficking to the cell surface regardless of whether or not they depend on furin cleavage for infectivity.

RESULTS

GBP5 expression reduces virion incorporation of glycoproteins that undergo furin-dependent processing

As a first step toward elucidating the anti-viral mechanism of action of GBP5, we determined the expression and inducibility of GBP5 in the Jurkat E6.1 human T-cell line, A549 lung epithelial cells, and HeLa cells by treating these cells with 10- or 100-ng/mL IFN-γ. As a control, the expression of the IFN-inducible gene STAT-1 was examined in parallel. In all cell lines tested, GBP5 expression was markedly induced by IFN-γ (Fig. 1A). We also observed strong IFN-induced expression of GBP5 in primary small airway epithelial cells, a target cell type for coronavirus infections (Fig. 1B). To measure GBP5 expression in primary human T cells, which serve as targets for HIV-1 infection *in vivo*, we left untreated or treated primary human peripheral blood mononuclear cells (PBMCs) with phytohemagglutinin P (PHA-P) and interleukin-2 (IL-2) and 100 ng/mL of IFN-γ (Fig. 1C). GBP5 expression was highly induced relative to unstimulated PBMCs. To avoid overexpression artifacts in the experiments that follow, we next sought to establish a range of GBP5 expression vector inputs in transfected HEK293T cells that recapitulate endogenous expression levels in relevant cell types. We then compared the expression of GBP5 in cultures of HEK293T cells transfected with 0.5, 0.75, or 1.0 µg of GBP5 expression vector with PBMCs from two donors activated with PHA-P and IL-2 and treated with 100 ng/mL of IFN-γ. This analysis allowed us to conclude that, when adjusted for the ~30% transfection efficiency (Fig. 1D), on a per-cell basis (normalized for tubulin), 0.5 µg of GBP5 expression vector provided a close match for levels of endogenous GBP5 expressed in activated PBMCs (Fig. 1E).

It has been shown that the expression of GBP5 in virus-producer cells reduces the infectivity of HIV-1 virions bearing HIV-1 Env or pseudotyped with the glycoprotein of rabies virus, European bat lyssavirus, IAV, or MLV (17, 18). However, the molecular mechanism by which GBP5 targets these viral glycoproteins is not well defined. As mentioned in the Introduction, it has been determined that GBP5 suppresses the activity of the cellular convertase furin, leading to reduced cleavage of viral glycoproteins and, hence, reduced viral infectivity (18). To confirm the ability of GBP5 to antagonize viral glycoproteins that undergo furin-dependent cleavage, we co-transfected HEK293T cells with the Env(–) pNL4-3 derivative pNL4-3/KFS (20) and MLV Env or an Env(–) luciferase-encoding pNL4-3 derivative pNL4-3.Luc.R-E- (21) (hereafter referred to as pNL4-3/Luc) and an expression vector for SARS-CoV-2 S from the Wuhan strain with or without GBP5 expression plasmid. For HIV-1 Env experiments, we used the full-length HIV-1 molecular clone pNL4-3 (22) with or without GBP5 expression plasmid. Virus-containing supernatants were harvested, normalized for reverse transcriptase (RT) activity, and used to infect the TZM-bl indicator cell line (23) or, in the case of the S protein pseudotypes, HEK293T cells stably expressing the human angiotensin-converting enzyme 2 (hACE2) receptor and transfected with transmembrane protease serine 2 (TMPRSS2). Consistent with previous reports (17, 18), the infectivity of particles bearing HIV-1 Env (Fig. 2A), MLV Env (Fig. 2B), or SARS-CoV-2 S (Fig. 2C) was reduced by GBP5 in a concentration-dependent manner.

We next investigated the ability of GBP5 to affect viral glycoprotein incorporation into virus particles. We analyzed cell- and virion-associated HIV-1 Env, MLV Env, and SARS-CoV-2 S glycoproteins by Western blot (Fig. 3). GBP5 caused a dose-dependent shift in the electrophoretic mobility of the HIV-1 surface Env glycoproteins gp120 and transmembrane glycoprotein gp41 (Fig. 3A), the MLV surface Env glycoprotein gp70 (Fig. 3B), and SARS-CoV-2 S2 (Fig. 3C) in cellular lysates without affecting Gag expression or processing. Notably, GBP5 strongly reduced virion incorporation of correctly sized mature glycoproteins (Fig. 3A through F). GBP5 expression also increased the levels of uncleaved gp160 in the virion fraction (Fig. 3A). Infectivity of particles bearing HIV-1 Env, MLV Env, or SARS-CoV-2 S correlated directly with the levels of virion-associated gp120, gp70, and S2, respectively (Fig. S1A through C). Altogether, these data demonstrate that,

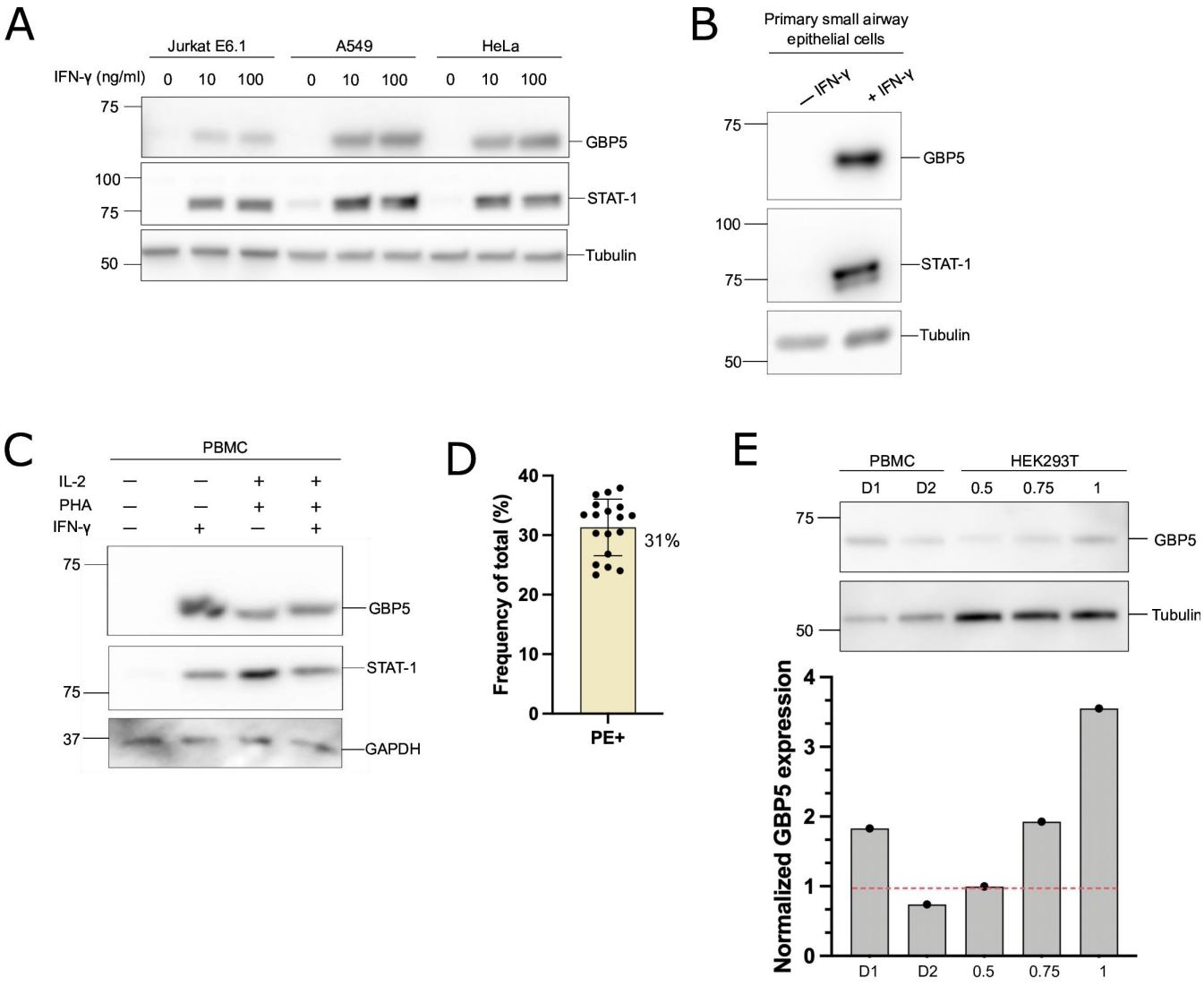

FIG 1 Establishment of physiologically relevant GBP5 expression levels in transfected HEK293T cells. (A) Jurkat E6.1 T-cells, lung epithelial A549 cells, and HeLa cells were untreated or treated with 10 or 100 ng/mL of IFN-γ for 24 h. (B) Primary small airway epithelial cells were untreated or treated with 100 ng/mL of IFN-γ for 24 h. (C) Non-activated human peripheral blood mononuclear cells (PBMCs) or PBMCs activated with phytohemagglutinin P (PHA-P) and interleukin-2 (IL-2) were untreated or treated with 100 ng/mL of IFN-γ for 24 h. (D) Transfection efficiency in HEK293T cells was determined by flow cytometry. HEK293T cells were transfected with GBP5 expression plasmid (0.5 µg). Two days post-transfection, cells were collected, fixed, and permeabilized. After permeabilization, cells were incubated with phycoerythrin (PE)-conjugated anti-HA.11 epitope tag antibody to detect GBP5. Frequency of the PE-positive population was determined with FlowJo version 10.9.0 software. Data shown are means ± SDs from 18 independent experiments. The average percentage of GBP5+ cells is shown to the right of the histogram. (E) PHA-P and IL-2-activated PBMCs were treated with 100-ng/mL IFN-γ for 24 h. Two PBMC donors were tested (D1 and D2); HEK293T cells were transfected with 0.5, 0.75, or 1.0 µg GBP5 expression vector. Cell lysates were prepared and subjected to Western blot analysis with anti-GBP5, anti-STAT-1, anti-GAPDH, or anti-alpha-tubulin. The mobility of molecular mass standards is shown on the left of each blot in kilodalton. To account for the approximately 30% transfection efficiency (D), the GBP5 signals in HEK293T cells were multiplied by three. (E) The GBP5 signal is presented as the GBP5:tubulin ratio, with the ratio for 0.5-µg GBP5 in HEK293T cells being set to 1. Protein bands were visualized using chemiluminescence with a Sapphire biomolecular imager (Azure Biosystems) and analyzed with ImageJ 1.53k software.

in a concentration-dependent manner, GBP5 impairs the infectivity of viruses bearing glycoproteins that undergo furin-dependent processing. Furthermore, the data show that GBP5 expression in virus-producer cells increases the electrophoretic mobility of mature glycoproteins and reduces their levels in virions.

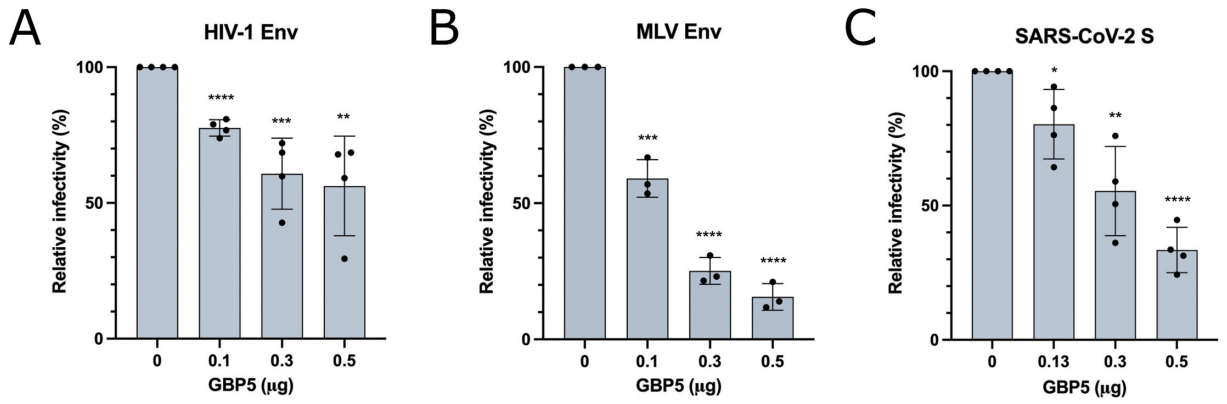

FIG 2 GBP5 expression reduces HIV-1 virion infectivity and the infectivity of HIV-1 particles pseudotyped with MLV Env or SARS-CoV-2 S. HEK293T cells were co-transfected with different quantities of a GBP5 expression vector, with total DNA held constant with empty vector control and (A) the pNL4-3 molecular clone (4 µg), (B) The Env-defective pNL4-3 derivative pNL4-3/KFS (3.3 µg) and MLV Env expression plasmid (0.6 µg), or (C) the Env(−) luciferase-encoding NL4-3-derived vector pNL4-3.Luc.R-E- (pNL4-3/Luc) (3 µg) and SARS-CoV-2 S (Wuhan strain) expression plasmid (1 µg). Two days post-transfection, virus supernatants were collected, normalized for RT activity, and used to infect TZM-bl cells (A and B) or HEK293T cells stably expressing hACE2 and transfected with TMPRSS2 expression plasmid (C). The infectivity in the absence of GBP5 is set at 100%. Data shown are means ± SDs from three independent experiments. Statistical significance (two-tailed unpaired *t*-test): **P* < 0.05, ***P* < 0.02, ****P* < 0.01, *****P* < 0.0001.

GBP5 expression reduces the cell-surface expression of HIV-1 Env and SARS-CoV-2 S

The Western blotting data presented above demonstrate that GBP5 expression disrupts virion incorporation of viral envelope glycoproteins, suggesting that GBP5 might alter the trafficking of these viral glycoproteins. It has been previously reported that exogenously expressed GBP5 partially co-localizes with the *trans*-Golgi marker TGN46 (18) and that SARS-CoV-2 S co-localizes with the ER marker calnexin in HEK293T cells in the presence of GBP5 (19). These results suggest that GBP5 expression may lead to the retention of viral glycoproteins in the ER or Golgi apparatus. To examine the effect of GBP5 on the expression of viral glycoproteins on the cell surface, we performed flow cytometry using HEK293T cells transfected with pNL4-3 or co-transfected with SARS-CoV-2 S expression vector and pNL4-3/KFS, with or without GBP5 expression plasmid. As a control, we used the isoprenylation-defective GBP5 mutant C583A (18, 24), which we confirmed to be inactive in virus infectivity assays (Fig. S2). As before, we also analyzed cell- and virion-associated proteins by Western blot (Fig. S3A and B). Our flow cytometry data show that in the presence of wild-type (WT) GBP5 but not the C583A GBP5 mutant, the cell-surface expression of HIV-1 Env (Fig. 4A) and SARS-CoV-2 S (Fig. 4B) is significantly reduced. These findings are consistent with the infectivity and Western blotting data presented above and indicate that reduced levels of mature glycoproteins in virions in the presence of GBP5 are associated with their reduced expression on the cell surface.

Overexpression of HIV-1 Env and SARS-CoV-2 S overcomes GBP5 restriction

To investigate the relationship between viral glycoprotein expression levels and GBP5-induced inhibition of cell-surface glycoprotein expression, we performed flow cytometry using HEK293T cells co-transfected with the HIV-1 Env expression vector pIIINL4env (25) or SARS-CoV-2 S expression vector and pNL4-3/KFS or pNL4-3/Luc, respectively, with or without GBP5 expression plasmid (WT or the inactive C583A mutant) (18, 24). The amount of pNL4-3/KFS and pNL4-3/Luc was kept constant, while the amounts of HIV-1 Env and SARS-CoV-2 S expression plasmids were varied to achieve a range of expression levels of these glycoproteins. Consistent with the above results with full-length pNL4-3 (Fig. 2A), we observed a significant reduction in cell-surface HIV-1 Env expression (Fig. 5A) and particle infectivity (Fig. 5B) in the presence of WT GBP5 when we used pIIINL4env and pNL4-3/KFS at a low (1:10) ratio. In contrast, there was no significant reduction in

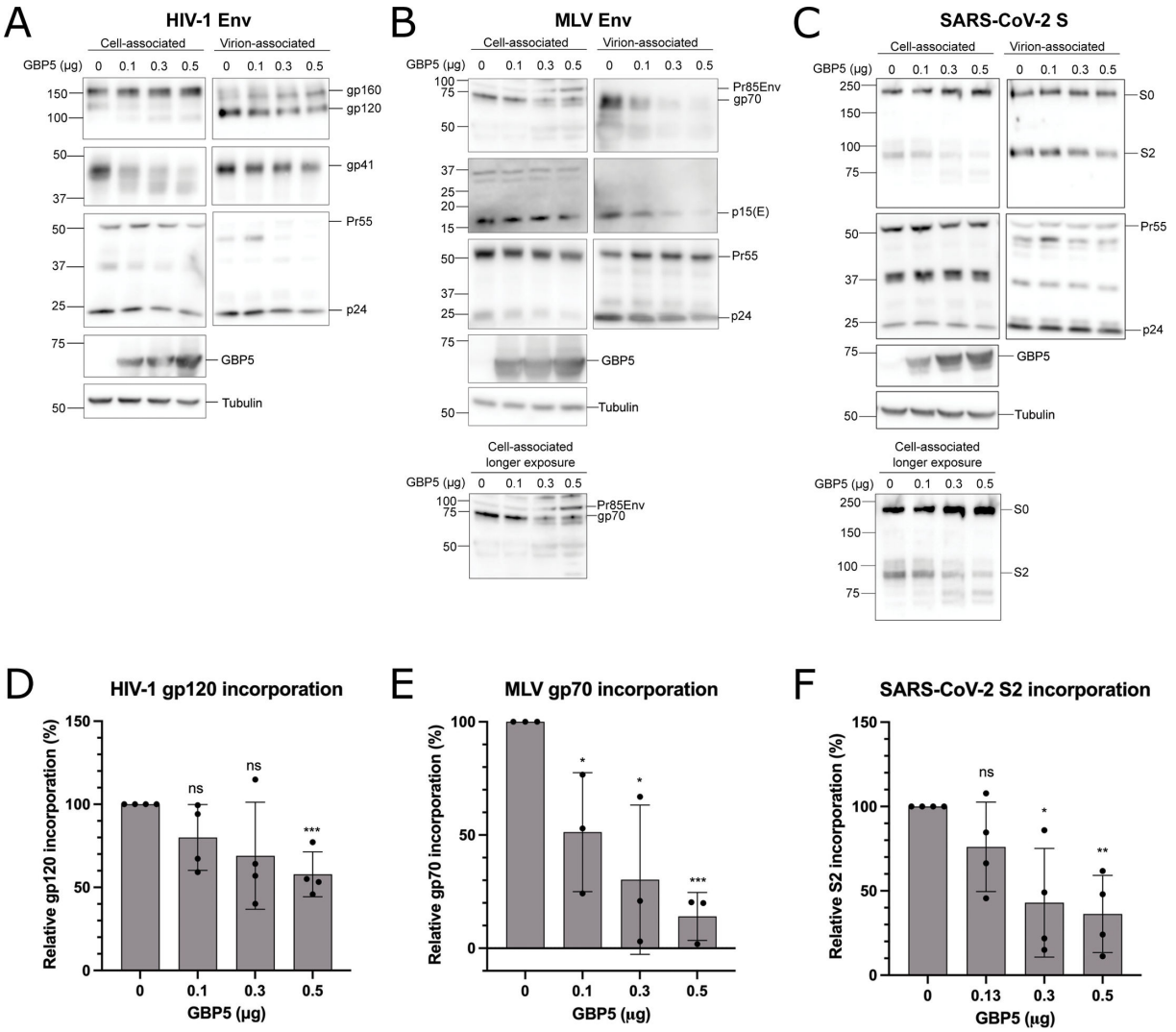

FIG 3 GBP5 expression increases the electrophoretic mobility of cell-associated HIV-1 Env, MLV Env, and SARS-CoV-2 S and reduces their incorporation into virions. HEK293T cells were co-transfected with varying quantities of a GBP5 expression vector, with total DNA held constant (at 0.5 µg) with empty vector control and (A) the pNL4-3 molecular clone (4 µg), (B) the Env-defective pNL4-3 derivative pNL4-3/KFS (3.3 µg) and MLV Env expression plasmid (0.6 µg), or (C) the Env(−) luciferase-encoding NL4-3-derived vector pNL4-3.Luc.R-E- (pNL4-3/Luc) (3 µg) and SARS-CoV-2 S expression plasmid (1 µg). Two days post-transfection, cell and virus lysates were prepared and subjected to Western blot analysis with anti-HIV-1 Ig to detect Gag proteins, anti-HIV-1 gp120, anti-HIV-1 gp41, anti-MLV gp70, anti-MLV p15(E), anti-SARS-CoV/SARS-CoV-2 S, anti-GBP5, or anti-alpha-tubulin. Positions of the HIV-1 Env glycoprotein precursor gp160, HIV-1 surface glycoprotein gp120, HIV-1 transmembrane glycoprotein gp41, Gag precursor Pr55Gag, p24 CA protein, MLV Env precursor Pr85Env, MLV surface Env glycoprotein gp70, MLV transmembrane protein p15(E), S precursor S0, and transmembrane spike glycoprotein S2 are indicated. The mobility of molecular mass standards is shown on the left of each blot in kilodaltons. The virion-associated levels of (D) HIV-1 gp120, (E) MLV gp70, and (F) SARS-CoV-2 S were quantified and normalized to virion-associated p24; values were set at 100% in the absence of GBP5. Analysis was performed with ImageJ 1.53k software. Data shown are means ± SDs from three to four independent experiments. Statistical significance (two-tailed unpaired *t*-test): **P* < 0.05, ***P* < 0.02, ****P* < 0.01. ns, not significant.

cell-surface levels of HIV-1 Env upon expression of WT GBP5 when we used pIIINL4env and pNL4-3/KFS at a threefold higher ratio (1:3) (Fig. 5C). The infectivity of HIV-1 virions was also not affected by the expression of WT GBP5 under these latter conditions (Fig. 5D). These results demonstrate that overexpression of HIV-1 Env can overcome GBP5 restriction. To confirm that HIV-1 Env glycosylation is not affected by GBP5 when pIIINL4env and pNL4-3/KFS are transfected at the higher ratio (1:3), we analyzed cell- and virion-associated proteins by Western blot. Consistent with the flow cytometry and infectivity data, WT GBP5 increased the electrophoretic mobility of gp120 and gp41 in cellular extracts when pIIINL4env and pNL4-3/KFS were co-transfected at a 1:10 but not

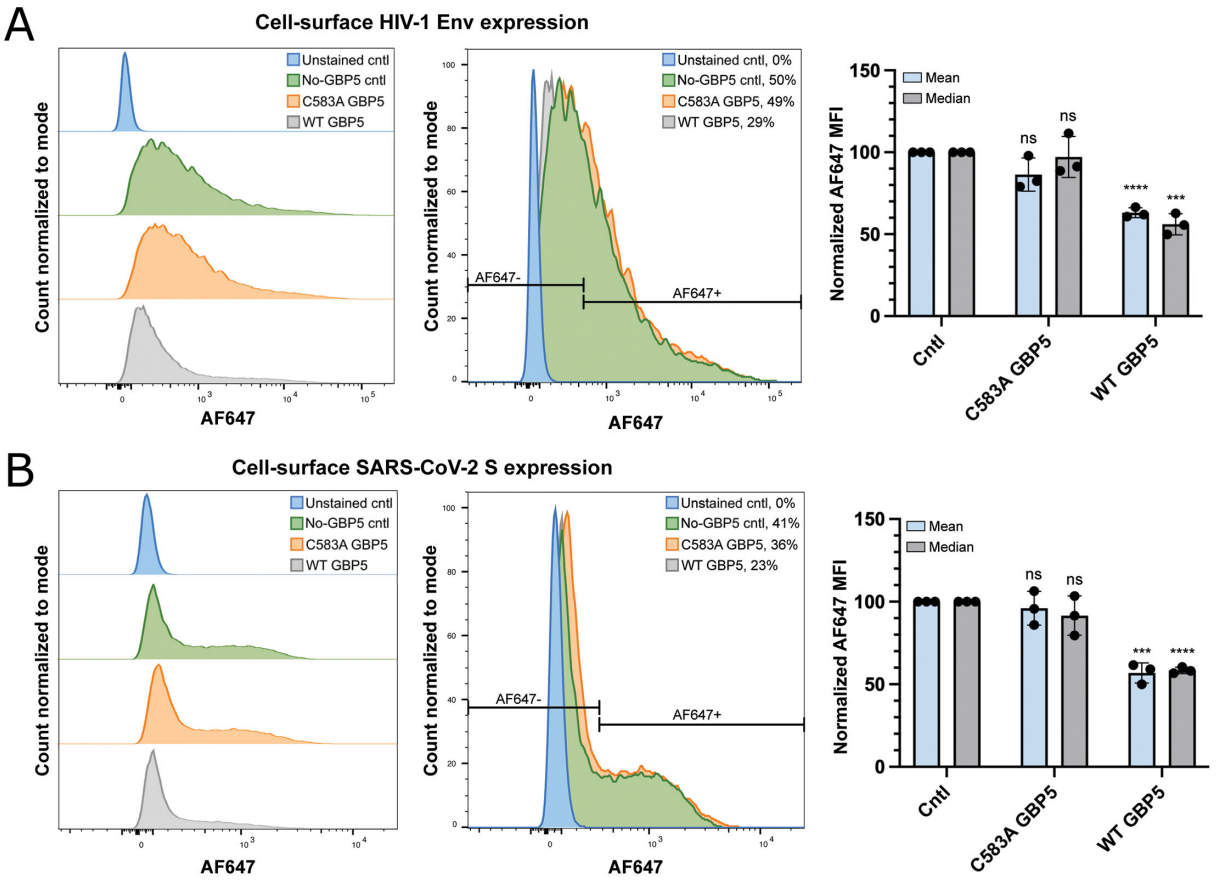

FIG 4 GBP5 reduces cell-surface HIV-1 Env and SARS-CoV-2 S expression. HEK293T cells were co-transfected with either wild-type (WT) GBP5 expression plasmid (0.5 µg) or the isoprenylation-deficient GBP5 mutant C583A (0.5 µg) and (A) the pNL4-3 molecular clone (4 µg) or (B) the Env(–) pNL4-3 derivative pNL4-3/KFS (3 µg) and SARS-CoV-2 S expression plasmid (1 µg). Two days post-transfection, cells were collected, incubated with anti-HIV-1 gp120 or Alexa Fluor 647-conjugated SARS-CoV-2 spike S1 subunit antibody, fixed, and permeabilized. After permeabilization, cells were incubated with goat anti-human antibody conjugated to Alexa Fluor 647 to stain HIV-1 gp120 and with PE-conjugated anti-HA.11 epitope tag antibody to detect GBP5. Histograms of HIV-1 Env- and SARS-CoV-2 S-positive Alexa Fluor 647 (AF647) expression were plotted in the absence of GBP5 (green) or in the presence of either C583A GBP5 (orange) or WT GBP5 (gray). Histogram of AF647 positivity of unstained cells (blue) was included as a control. Mean and median fluorescence intensity (MFI) of HIV-1 Env and SARS-CoV-2 S cell-surface expression was calculated with FlowJo version 10.9.0 software. The MFI in the absence of GBP5 is set at 100%. Data shown are means ± SDs from three independent experiments. Statistical significance (two-tailed unpaired *t*-test): ***$P < 0.01$; ****$P < 0.0001$. ns, not significant.

1:3 ratio (Fig. S4A). Furthermore, WT GBP5 strongly reduced virion incorporation of correctly sized gp120-gp41 trimers while increasing virion-associated levels of the gp160 glycoprotein precursor at the 1:10 but not 1:3 ratio (Fig. S4B). Together, these results demonstrate that HIV-1 Env overexpression can overcome GBP5 restriction. This result is consistent with an earlier report that HIV-1 can achieve partial resistance to GBP5 by inactivating the *vpu* gene, thereby increasing Env expression (17).

Experiments similar to those presented above for HIV-1 Env were performed with SARS-CoV-2 S to investigate whether varying levels of SARS-CoV-2 S expression affect GBP5-mediated restriction. Cells were transfected with a range of SARS-CoV-2 S expression vector inputs while keeping the amount of pNL4-3/Luc constant. In the case of SARS-CoV-2 S expression plasmid and pNL4-3/Luc at a low (1:5) ratio, we observed a significant reduction in S cell-surface expression upon GBP5 expression (Fig. 5E) and a ~ 90% reduction in pseudotyped particle infectivity (Fig. 5F). In contrast, when SARS-CoV-2 S expression plasmid and pNL4-3/Luc were co-transfected at a higher (1:2 or 1:1) ratio, we did not observe a significant difference in S cell-surface expression upon GBP5 expression (Fig. 5G; Fig. S4C). Consistent with this result, pseudotyped particle infectivity was not affected by expression of WT GBP5 when SARS-CoV-2 S expression plasmid and

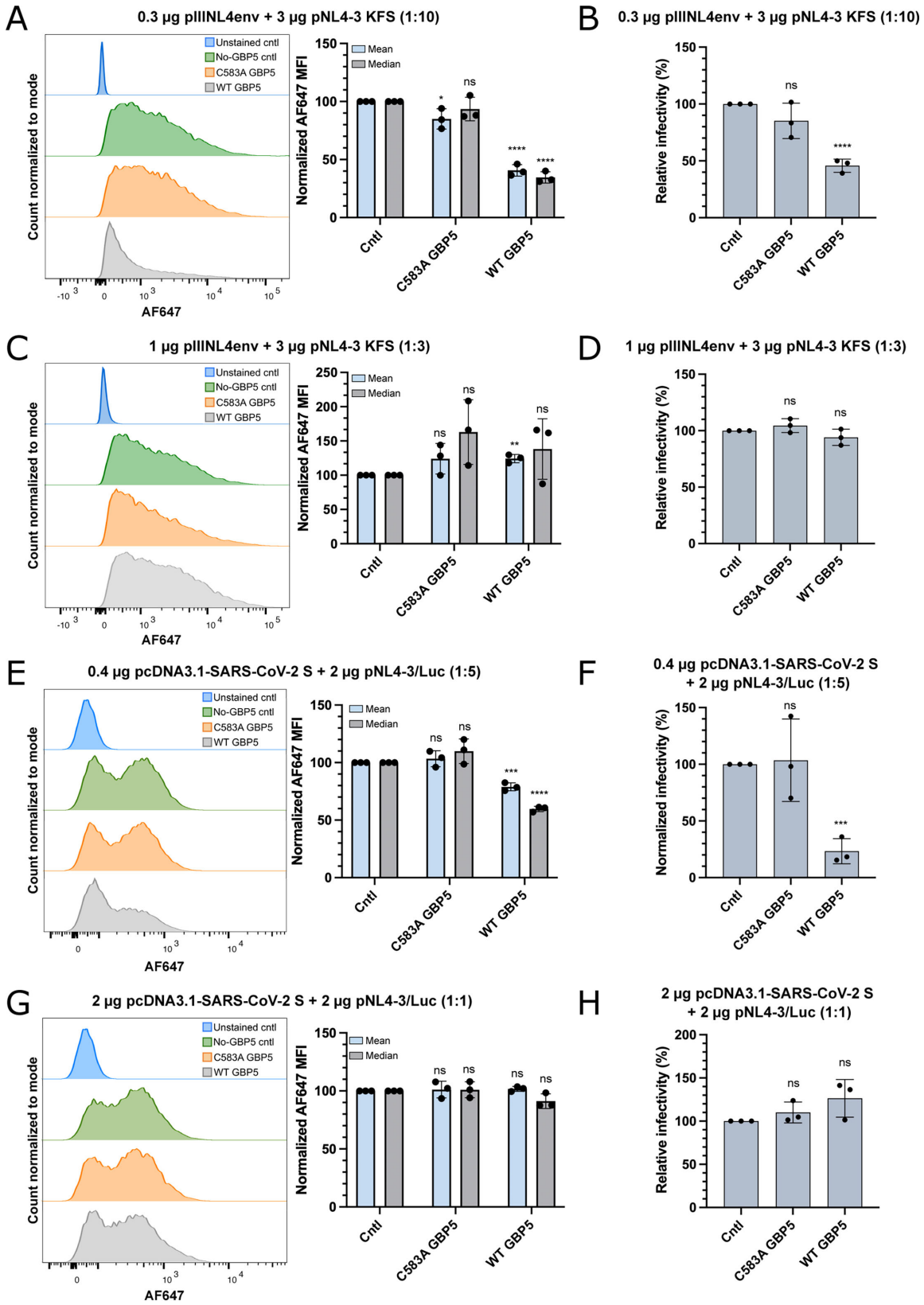

FIG 5 Overexpression of HIV-1 Env and SARS-CoV-2 S confers GBP5 resistance. HEK293T cells were co-transfected with either WT GBP5 expression plasmid (0.5 µg) or the isoprenylation-deficient GBP5 mutant C583A (0.5 µg) and the Env-defective pNL4-3 derivative pNL4-3/KFS and HIV-1 Env expression plasmid at a ratio of 1:10 (A and B) or 1:3 (C and D), or Env(–) luciferase-encoding NL4-3-derived vector pNL4-3.Luc.R-E- (pNL4-3/Luc) and SARS-CoV-2 S expression plasmid

(Continued on next page)

Fig 5 (Continued)

at a ratio of 1:5 (E and F) or 1:1 (G and H). Two days post-transfection, cells were collected, incubated with anti-HIV-1 gp120 or AF647-conjugated SARS-CoV-2 spike S1 subunit antibody, fixed, and permeabilized. After permeabilization, cells were incubated with goat anti-human antibody conjugated to AF647 to stain HIV-1 gp120 and with PE-conjugated anti-HA.11 epitope tag antibody to detect GBP5. Histograms of HIV-1 Env- (A and C) and SARS-CoV-2 S- (E and G) positive expression were plotted in the absence of GBP5 (green) or in the presence of either C583A GBP5 (orange) or WT GBP5 (gray). Histogram of AF647 positivity of unstained cells (blue) was included as a control. Mean and median fluorescence intensity (MFI) of HIV-1 Env and SARS-CoV-2 S cell-surface expression was calculated with FlowJo 10.9.0 software. The MFI in the absence of GBP5 is set at 100%. Data shown are means ± SDs from three independent experiments. Statistical significance (two-tailed unpaired *t*-test): *$P < 0.05$; **$P < 0.02$; ****$P < 0.0001$. Virus supernatants were collected, normalized for RT, and used to infect TZM-bl cells (B and D) or HEK293T cells stably expressing hACE2 and transfected with TMPRSS2 expression plasmid (F and H). The infectivity in the absence of GBP5 is set at 100%. Data shown are means ± SDs from three independent experiments. Statistical significance (two-tailed unpaired *t*-test): ***$P < 0.01$; ****$P < 0.0001$. ns, not significant.

pNL4-3/Luc were co-transfected at a ratio of 1:2 (Fig. S4D) or 1:1 (Fig. 5H). To confirm that glycosylation of SARS-CoV-2 S is not affected by GBP5 when SARS-CoV-2 S expression plasmid and pNL4-3/Luc are transfected at a ratio of 1:2 or 1:1, we analyzed cell- and virion-associated proteins by Western blot. As shown above, WT GBP5 increased the electrophoretic mobility of S2 from cellular extracts (Fig. S4E) and strongly reduced virion incorporation of correctly sized S2 (Fig. S4F) at the 1:5 ratio. Increasing the ratio to 1:2 had a lesser effect on S2 glycosylation, and no effect on S2 incorporation was observed at the 1:2 or 1:1 ratio (Fig. S4E and F). Taken together, these results demonstrate that increasing HIV-1 Env or SARS-CoV-2 S expression can overcome GBP5-mediated restriction.

GBP5 targets viral glycoproteins that do not undergo furin-dependent processing

To investigate whether GBP5 expression exerts anti-viral activity on viral glycoproteins that are not cleaved by furin, we co-transfected HEK293T cells with VSV-G or SARS-CoV S expression vectors and the Env(–) pNL4-3 derivatives pNL4-3/KFS or pNL4-3/Luc, respectively, with or without GBP5 expression plasmid. Virus-containing supernatants were harvested, normalized for RT activity, and used to infect the TZM-bl indicator cell line or, in the case of the S protein pseudotypes, HEK293T cells stably expressing hACE2 and transfected with TMPRSS2. We observed that the infectivity of particles bearing SARS-CoV S, which has been reported to require cathepsin L host protease priming (26), was reduced in a GBP5 concentration-dependent manner (Fig. 6A). In contrast to previous reports (18, 19), GBP5 expression in the virus-producer cell also impaired the infectivity of particles bearing VSV-G, which does not require protease priming (Fig. 6B). Western blots of cell lysates indicated that GBP5 expression causes a dose-dependent shift in the electrophoretic mobility of SARS-CoV S (Fig. 6C) and VSV-G (Fig. 6D). GBP5 reduced the virion incorporation of correctly sized mature SARS-CoV S and VSV-G (Fig. 6C through F). As expected from these results, the infectivity of particles bearing SARS-CoV S or VSV-G correlated strongly with the virion-associated levels of these glycoproteins (Fig. S1D and E). Flow cytometry analysis showed that in the presence of WT GBP5 but not the C583A GBP5 mutant, cell-surface expression of SARS-CoV S is significantly reduced (Fig. 6G). Altogether, these results demonstrate that GBP5 expression in the virus-producer cell antagonizes viral glycoproteins independently of whether they undergo activation by furin.

GBP5 disrupts viral glycoprotein glycosylation and can antagonize viral glycoproteins that depend on furin cleavage without blocking furin processing

The Western blot and flow cytometry data presented above demonstrate that GBP5 expression increases the electrophoretic mobility and reduces the cell-surface expression of the viral glycoproteins tested, suggesting that GBP5 expression in virus-producer cells interferes with the glycosylation and trafficking of viral glycoproteins, ultimately

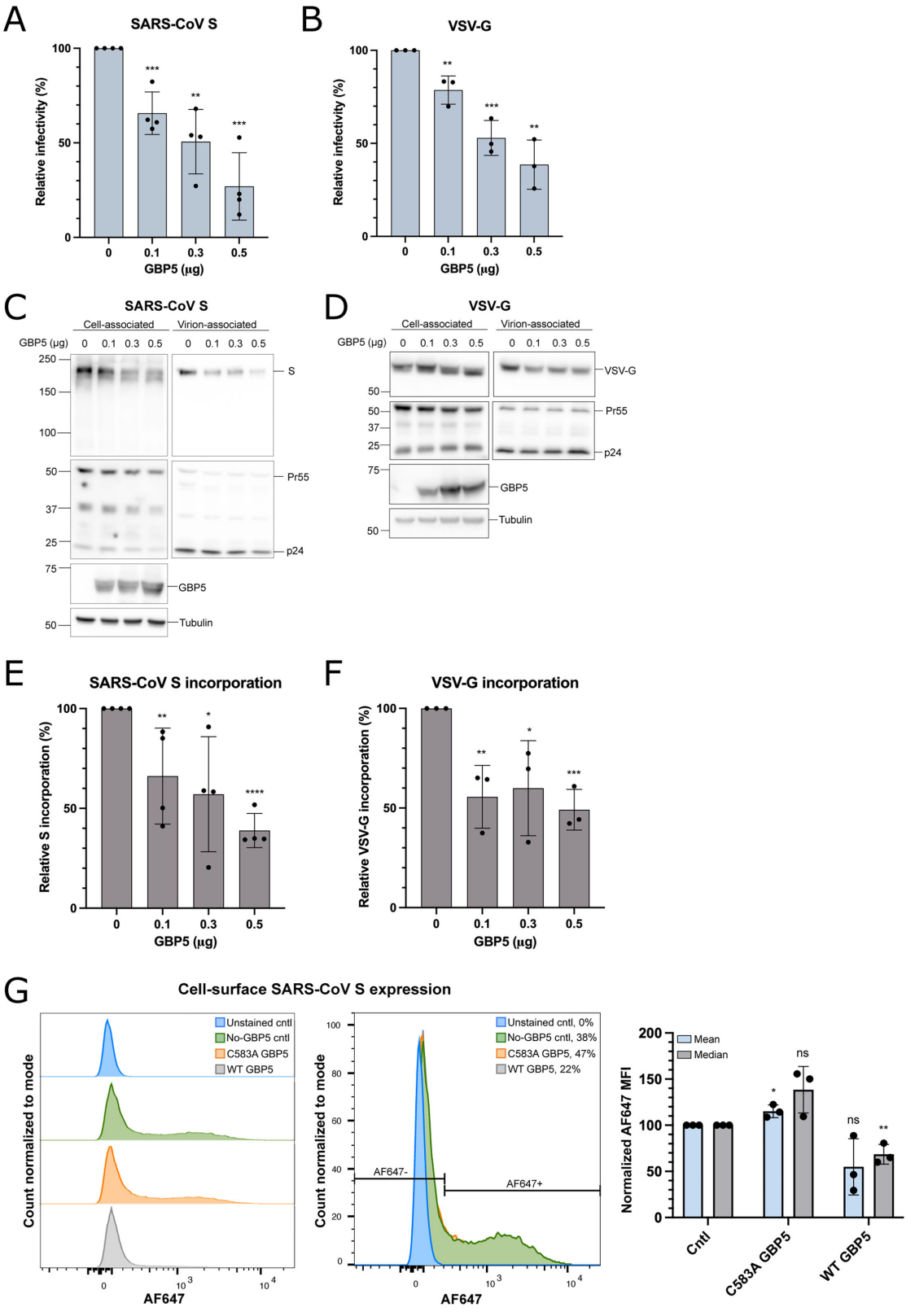

FIG 6 GBP5 reduces the infectivity of HIV-1 virions pseudotyped with SARS-CoV S and VSV-G, inhibits the virion incorporation of SARS-CoV S and VSV-G, and reduces the cell-surface expression of SARS-CoV S. HEK293T cells were co-transfected with varying quantities of a GBP5 expression vector, with total DNA held constant with empty control vector (0.5 µg total), and (A) Env(–) luciferase-encoding NL4-3-derived vector pNL4-3.Luc.R-E- (pNL4-3/Luc) (3 µg) and SARS-CoV

(Continued on next page)

Fig 6 (Continued)

S expression plasmid (1 µg), or (B) the Env(−) pNL4-3 derivative pNL4-3/KFS (4 µg) and VSV-G expression plasmid (0.5 µg). Two days post-transfection, virus supernatants were collected, normalized for RT activity, and used to infect TZM-bl (A) or HEK293T cells stably expressing hACE2 and transfected with TMPRSS2 expression plasmid (B). The infectivity in the absence of GBP5 is set at 100%. Data shown are means ± SDs from three to four independent experiments. Statistical significance (two-tailed unpaired *t*-test): $^{**}P < 0.02$; $^{***}P < 0.01$. Cell and virus lysates of (C) SARS-CoV S- and (D) VSV-G-pseudotyped virions were prepared 2 days post-transfection and subjected to Western blot analysis with anti-HIV-1 Ig to detect Gag proteins, anti-SARS-CoV/SARS-CoV-2 S, anti-VSV-G, anti-GBP5, or anti-alpha-tubulin. The mobility of molecular mass standards is shown on the left of each blot in kilodalton. The levels of virion-associated (E) SARS-CoV S and (F) VSV-G were quantified and normalized to virion-associated p24; values were set at 100% in the absence of GBP5. Analysis was performed with ImageJ 1.53k software. Data shown are means ± SDs from three to four independent experiments. Statistical significance (two-tailed unpaired *t*-test): $^{*}P < 0.05$; $^{**}P < 0.02$; $^{***}P < 0.01$; $^{****}P < 0.0001$. (G) HEK293T cells were co-transfected with either WT GBP5 or the isoprenylation-deficient mutant C583A (0.5 µg), Env(−) luciferase-encoding NL4-3-derived vector pNL4-3.Luc.R-E- (pNL4-3/Luc) (3 µg), and SARS-CoV S expression plasmid (1 µg). Two days post-transfection, cells were collected, incubated with AF647-conjugated SARS-CoV-2 spike S1 subunit antibody, fixed, and permeabilized. After permeabilization, cells were incubated with PE-conjugated anti-HA.11 epitope tag antibody to detect GBP5. Histograms of SARS-CoV S-positive expression were plotted in the absence of GBP5 (green) or in the presence of either C583A GBP5 (orange) or WT GBP5 (gray). Histogram of AF647 positivity of unstained cells (blue) was included as a control. Mean and median fluorescence intensity (MFI) of SARS-CoV S cell-surface expression was calculated with FlowJo version 10.9.0 software. The MFI in the absence of GBP5 is set at 100%. Data shown are means ± SDs from three independent experiments. Statistical significance (two-tailed unpaired *t*-test): $^{*}P < 0.05$; $^{**}P < 0.02$. ns, not significant.

reducing their levels in virions and inhibiting particle infectivity. To determine the effect of GBP5 expression on glycoprotein glycosylation, we treated virus-producing cell lysates with peptide-*N*-glycosidase F (PNGase F), which removes *N*-linked oligosaccharides from glycoproteins. PNGase F treatment abolished the GBP5-mediated shift in the electrophoretic mobility of HIV-1 gp120 and gp41 (Fig. 7A), MLV gp70 (Fig. 7B), SARS-CoV-2 S2 (Fig. 7C), SARS-CoV S (Fig. 7D), and VSV-G (Fig. 7E). These results indicate that GBP5 indeed affects *N*-linked protein glycosylation and/or glycan modification, as has been shown before for HIV-1 and MLV Env (17) and SARS-CoV-2 (19). Furthermore, PNGase F data obtained with SARS-CoV S and VSV-G further demonstrate that GBP5 affects glycoproteins that do not undergo furin-dependent cleavage.

Previous studies showed that GBP5 suppresses the activity of furin, thereby inhibiting the infectivity of viral particles bearing glycoproteins that require furin cleavage (18). However, the results of this study show that GBP5 expression in virus-producer cells interferes with glycosylation and trafficking of glycoproteins regardless of whether they depend on furin cleavage for infectivity. To measure the effect of GBP5 expression on furin cleavage of viral glycoproteins, we quantified the ratios of cell-associated HIV-1 gp160 to gp120, MLV Pr85Env to gp70, and SARS-CoV-2 S0 to S2 from the experiments presented in Fig. 3. This quantification showed that when only fully glycosylated HIV-1 gp120 (Fig. 8A), MLV gp70 (Fig. 8B), or SARS-CoV-2 S2 (Fig. 8C) are quantified (indicated by # in Fig. 8A through C), there appears to be a GBP5 concentration-dependent decrease in furin cleavage. However, when the quantification includes furin-cleaved but mobility-shifted species (indicated by ##), a significant difference in furin-mediated glycoprotein cleavage is not observed. These data demonstrate that, under the conditions used here, GBP5 expression in virus-producer cells does not impair furin-dependent cleavage of HIV-1 Env, MLV Env, or SARS-CoV-2 S but rather shifts their mobility on sodium dodecyl sulfate-polyacrylamide gel electrophoresis (SDS-PAGE). Note that in Fig. 8A through C, blots from Fig. 3 are reproduced for ease of viewing.

To support these data, we also quantified the PNGase F-treated, glycan-stripped forms of HIV-1 gp160 and gp120, MLV Pr85Env and gp70, and SARS-CoV-2 S0 and S2 from the experiment presented in Fig. 7 to measure protein processing efficiency in the absence or presence of GBP5. Consistent with the analysis shown in Fig. 8A through C, the results of this quantification also showed no significant difference in glycoprotein processing upon expression of GBP5 (Fig. 8D through F). Note that in Fig. 8D through F, blots from Fig. 7 are reproduced for ease of viewing, with the relevant lanes highlighted with boxes. Altogether, these data show that GBP5 expression in virus-producer cells

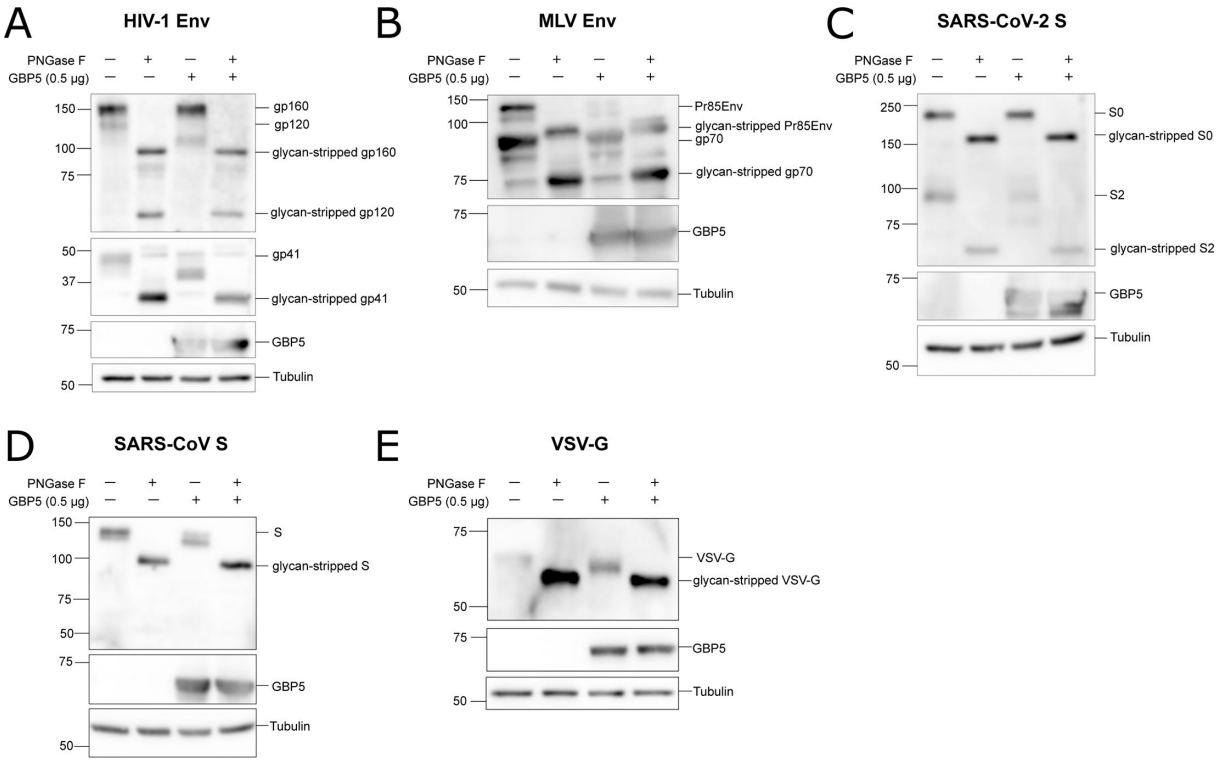

FIG 7 GBP5 reduces the glycosylation of HIV-1 Env, MLV Env, SARS-CoV-2 S, SARS-CoV S, and VSV-G. HEK293T cells were co-transfected with varying amounts of a GBP5 expression vector, with the total DNA held constant with empty vector (0.5 µg total), and (A) pNL4-3 (4 µg), (B) the Env(–) pNL4-3 derivative pNL4-3/KFS (3 µg) and MLV Env expression plasmid (0.6 µg), (C) Env(–) luciferase-encoding NL4-3-derived vector pNL4-3.Luc.R-E- (pNL4-3/Luc) (3.3 µg) and SARS-CoV-2 S expression plasmid (1 µg), (D) Env(–) luciferase-encoding NL4-3-derived vector pNL4-3.Luc.R-E- (pNL4-3/Luc) (3.3 µg) and SARS-CoV S expression plasmid (1 µg), or (E) the Env(–) pNL4-3 derivative pNL4-3/KFS (4 µg) and VSV-G expression plasmid (0.5 µg). Two days post-transfection, cell lysates were prepared and treated with PNGase F before being subjected to Western blot analysis with anti-HIV-1 gp120, anti-HIV-1 gp41, anti-MLV gp70, anti-SARS-CoV/SARS-CoV-2 S, anti-VSV-G, anti-GBP5, or anti-alpha-tubulin. The positions of the glycan-stripped viral glycoproteins in the PNGaseF-treated samples are indicated. The mobility of molecular mass standards is shown on the left of each blot in kilodalton.

can impair glycoprotein incorporation and particle infectivity without interfering with furin-dependent processing.

The analyses presented above have focused on viral glycoproteins. To determine whether GBP5 expression also targets a cellular glycoprotein, we expressed CD4 in HEK293T cells with and without GBP5. As observed for the viral glycoproteins tested, Western blot analysis indicated that GBP5 expression shifted the electrophoretic mobility of CD4 (Fig. S5). These results indicate that GBP5 expression affects the trafficking/glycosylation not only of viral glycoproteins but also of a cellular glycoprotein.

DISCUSSION

In this study, we examined the ability of GBP5 to antagonize a wide range of viral fusion glycoproteins, specifically, HIV-1 and MLV Env, SARS-CoV and SARS-CoV-2 S, and VSV-G. Expression of GBP5 in virus-producer cells interfered with viral glycoprotein glycosylation and incorporation into viral particles and reduced the infectivity of viruses bearing each of the glycoproteins tested. Moreover, expression of GBP5 in virus-producer cells reduced the cell-surface expression of HIV-1 Env and SARS-CoV and SARS-CoV-2 S. The cleavage of glycoproteins that undergo furin-mediated cleavage (HIV-1 Env, MLV Env, and SARS-CoV-2 S) was not affected by GBP5 expression; rather, under the experimental conditions used, the primary mechanism of GBP5 inhibition appears to be related to the glycosylation and trafficking of viral glycoproteins to the plasma membrane.

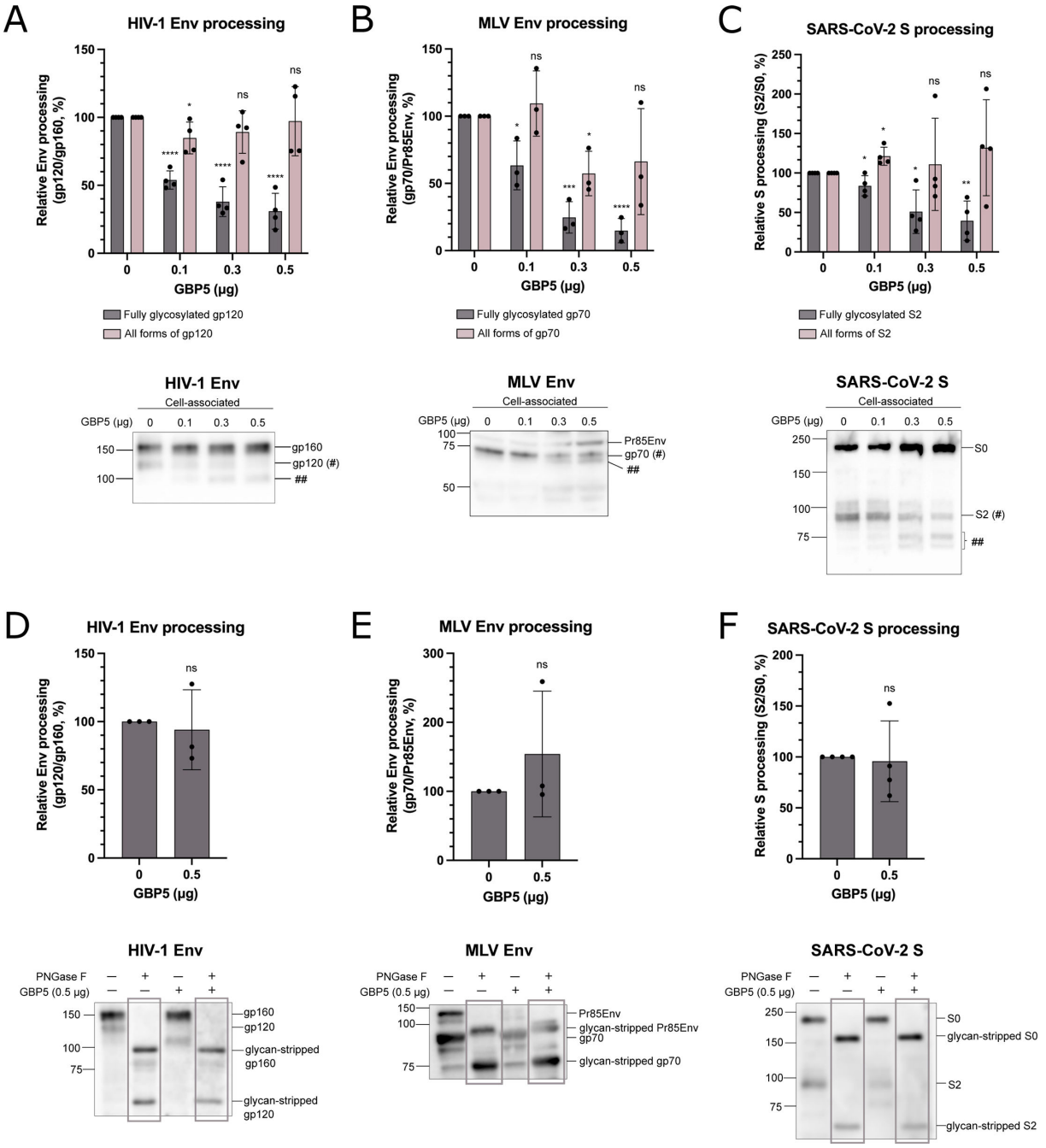

FIG 8 GBP5 does not impair the processing of HIV-1 Env, MLV Env, or SARS-CoV-2 S glycoproteins under the conditions tested. Quantification of the ratios of cell-associated (A) HIV-1 gp160/gp120, (B) MLV Pr85Env/gp70, and (C) SARS-CoV-2 S0/S2 in the presence of varying amounts of GBP5 expression plasmid (0–0.5 μg) is shown. Quantification included only fully glycosylated forms of gp120, gp70, or S2 (dark bars) or fully glycosylated plus the more rapidly migrating, less-glycosylated forms (light bars). Blots below the graphs are reproduced from Fig. 3 for ease of viewing; fully glycosylated forms of gp120, gp70, and S2 are denoted by #; lower-molecular-weight (less glycosylated) species are indicated by ##. Quantification of the ratios of cell-associated (D) HIV-1 gp160/gp120, (E) MLV Pr85Env/gp70, and (F) SARS-CoV-2 S0/S2 from PNGaseF-treated samples in the absence or presence of GBP5 expression plasmid (0.5 μg). Blots are reproduced from Fig. 7 for ease of viewing, with the bands quantified in the graphs boxed in the blots. Analysis was performed with ImageJ 1.53k software. Glycoprotein processing in the absence of GBP5 is set at 100%. Data shown are means ± SDs from three to four independent experiments. Statistical significance (two-tailed unpaired *t*-test): **P* < 0.05; ***P* < 0.02; ****P* < 0.01; *****P* < 0.0001. ns, not significant.

Previous studies demonstrated that GBP5 expression in the virus-producer cell reduces the infectivity of SARS-CoV-2 virions (19) and HIV-1 virions bearing either HIV-1

or MLV Env (17, 18). The overexpression of GBP5 in HEK293T cells, or IFN-γ stimulation of parental but not GBP5 knockout THP-1 cells, was shown to significantly reduce the infectivity of virions bearing glycoproteins that require furin-dependent activation but not those bearing VSV-G, which does not undergo cleavage by furin (18). In the current study, we confirmed that GBP5 expression reduces the glycosylation of glycoproteins that undergo furin-dependent cleavage (e.g., HIV-1 and MLV Env and SARS-CoV-2 S) and their incorporation into viral particles. However, quantification of our Western blot data did not show a significant reduction in furin-mediated cleavage of HIV-1 Env, MLV Env, or SARS-CoV-2 S when less-glycosylated species were included in the quantification (Fig. 8). We also show that GBP5 expression reduces the glycosylation, cell-surface expression, and pseudotype particle incorporation of the furin-independent viral glycoprotein SARS-CoV S. Moreover, we show that GBP5 reduces the glycosylation and incorporation of VSV-G (Fig. 6), which is not activated by host protease cleavage, and reduces the infectivity of VSV-G-bearing particles. This observation contrasts with the finding of Krapp et al. (17) that GBP5 does not impair the infectivity of VSV-G-bearing particles (17). Finally, we also show that GBP5 expression increases the electrophoretic mobility of the cellular protein CD4 (Fig. S5), indicating that effects of GBP5 on glycosylation/trafficking are not limited to viral glycoproteins. Thus, while the results presented here are largely in agreement with those reported in previous studies, a notable difference is that the activity of GBP5 observed under the conditions used here extended to glycoproteins that do not undergo cleavage by furin or furin-related proteases. This difference likely relates to the relative expression levels of GBP5 and the glycoproteins under study, as we demonstrated that GBP5-mediated antagonism could be overcome by higher viral glycoprotein expression levels. It is worth noting that the levels of GBP5 achieved in the transient transfections in our study match those measured in relevant IFN-γ-stimulated cells (see below).

Our results show a broad anti-viral activity of GBP5 against the glycoproteins from three human viral pathogens—HIV-1, SARS-CoV-2, and SARS-CoV—and two primarily animal pathogens, MLV and VSV. GBP5 targeting of HIV-1 and MLV Env (17, 18) and, very recently, SARS-CoV-2 S (19) has been reported. HIV-1 replicates predominantly in CD4+ T cells and also infects monocyte-derived macrophages (MDMs) (27, 28). MLV targets mainly cells of the hematopoietic and lymphoid systems (29). SARS-CoV and SARS-CoV-2, like other coronaviruses, target airway epithelial cells and other cell types (30). VSV typically replicates in cells of the oral mucosa, although VSV-G confers very broad tissue tropism (31). This raises the question of whether the levels of GBP5 expression achieved in the experiments described here are physiologically relevant. We demonstrated that IFN-γ stimulates GBP5 expression in Jurkat E6.1 T-cells, HeLa cells, and airway epithelial A549 cells, as well as in human PBMCs and primary small airway epithelial cells. In this study, we relied extensively on expressing GBP5 exogenously to evaluate its effect on viral fusion glycoprotein glycosylation and incorporation. The endogenous expression of GBP5 in IFN-γ-treated PBMCs, measured as a ratio to tubulin, was comparable to, or even higher than, the exogenous expression of 0.5 µg GBP5 in HEK293T cells. These results demonstrate that the levels of GBP5 expression achieved in this study are physiologically relevant at least in cell culture systems. These results also raise a question of whether endogenous GBP5 expression in IFN-γ-treated primary T cells would impose a stronger anti-viral response compared to exogenous GBP5 expression in HEK293T cells, given that Env expression in likely higher in transfected HEK293T cells than in infected T cells. Indeed, a significant increase in the yield of infectious HIV-1 upon GBP5 knockdown in MDMs and THP-1 cells has been reported (17, 18). Ongoing studies using PBMCs will examine the impact of GBP5 knockout on HIV-1 infectivity in primary T cells following IFN-γ stimulation.

A limitation of this study is that we used HIV-1 virions pseudotyped with either SARS-CoV or SARS-CoV-2 S and measured S incorporation into HIV-1 particles rather than bona fide coronavirus particles. Unlike HIV-1, β-coronaviruses like SARS-CoV and SARS-CoV-2 exit cells through the lysosomal exocytic pathway rather than via direct

budding from the plasma membrane (32). Their egress pathway begins with particle budding into the lumen of the ER and the ER-Golgi intermediate compartment (ERGIC). From the ER/ERGIC, β-coronaviruses traffic to the Golgi apparatus and TGN for glycosylation and other post-translational modification. Therefore, GBP5 is likely to interfere with the glycosylation of the S protein in the context of bona fide SARS-CoV and SARS-CoV-2 virions and consequently to affect their infectivity. Indeed, Mesner et al. (19) showed that GBP5 inhibits SARS-CoV-2 S incorporation and particle infectivity in the context of SARS-CoV-2 virus-like particles (19). Another limitation of this study is that we tested Env from only a CXCR4-tropic strain of HIV-1. However, previous studies reported significant increases in infectious yield of CCR5-tropic HIV-1 Bal and AD8 upon GBP5 siRNA knockdown in human macrophages, demonstrating that CCR5-tropic HIV-1 Env is also antagonized by GBP5 (17).

The type I IFN (IFN-I) response is crucial in the host anti-viral defense against viral infections (33, 34). A recent publication highlighted the importance of the IFN-I response in immune protection against SARS-CoV-2 by establishing a link between life-threatening COVID-19 symptoms and loss-of-function mutations in IFN-I-related genes (35). Another recent finding showed that a different ISG, IFITM3, disrupts the glycosylation of VSV-G (36), suggesting that glycosylation might serve as a broadly effective mechanism of IFN-mediated anti-viral defense. Expression of GBP5 in virus-producer cells inhibited every viral glycoprotein examined in this study, raising important questions about the impact of GBP5 expression on cellular proteins. A previous study demonstrated that proteolytic processing of the furin substrates glypican-3 and matrix metalloproteinase-14 is significantly reduced in the presence of GBP5 (18), and we show here that the glycosylation of CD4 is affected by GBP5 expression. Thus, viral glycoproteins are not uniquely susceptible to GBP5 antagonism, but rather, this protein likely generally influences protein glycosylation and trafficking pathways. GBP5 could directly interfere with the glycosylation machinery or the enzymes involved in glycan modification (e.g., conversion of high-mannose side chains to the larger, complex, or hybrid side chains) (37) or could impede the trafficking of glycoproteins through the Golgi compartments where high-mannose side chains are converted to complex/hybrid side chains. In either case, failure to modify high-mannose side chains to complex/hybrid types likely explains the shift in glycoprotein mobility observed here and in previous studies (17–19). While this paper was in preparation, Wang et al. (38) deposited a paper in bioRxiv reporting that GBP5 binds the host oligosaccharyltransferase complex, thereby inhibiting the glycosylation of SARS-CoV-2 S and other viral glycoproteins (38). These results are consistent with the findings reported here that GBP5 inhibits the glycosylation of a range of viral and cellular glycoproteins. Further studies are needed to elucidate the exact mechanism by which GBP5 and other members of the GBP family (like GBP2, which also has broad anti-viral activity [18]) alter the trafficking of glycoproteins to the PM. While it might appear to be disadvantageous for cells to express a protein that globally disrupts a crucial cellular pathway, cells maintain the expression of GBP5 (and other family members) at a low level until the IFN response is triggered by pathogen invasion. Ongoing work using fully infectious viruses in animal models is investigating mechanisms by which viruses counteract the anti-viral activity of GBP5 and elucidating its relevance *in vivo*.

MATERIALS AND METHODS

Cell culture

HEK293T cells (obtained from the American Type Culture Collection [ATCC]), HEK293T cells stably expressing hACE2 receptor (BEI Resources, catalog number NR-52511), A549 human lung epithelial cells (obtained from the ATCC), HeLa cells (obtained from the ATCC), and TZM-bl cells (obtained from J.C. Kappes, X. Wu, and Tranzyme, Inc. through the NIH AIDS Reagent Program [ARP], Germantown, MD) were maintained in Dulbecco modified Eagle medium containing 10% (vol/vol) fetal bovine serum (FBS, HyClone) and

2 mM glutamine at 37°C with 5% CO_2. Primary small airway epithelial cells (obtained from the ATCC) were cultured in airway epithelial cell basal medium (ATCC) supplemented with bronchial epithelial growth kit (ATCC, PCS-300-040) at 37°C with 5% CO_2. The Jurkat E6.1 T-cell line (obtained from the ATCC) was cultured in RPMI-1640 medium with 10% (vol/vol) FBS at 37°C with 5% CO_2. Primary PBMCs were obtained from healthy volunteers from the National Cancer Institute (NCI)-Frederick Research Donor Program. The PBMCs were enriched from whole blood using the Histopaque procedure (Sigma-Aldrich). Cells were then stimulated with 2-µg/mL PHA-P (MilliporeSigma, catalog no. L1668) and 50-U/mL IL-2 (Roche, catalog no. Ro 23-6019) for 3 days and cultured in RPMI with 10% (vol/vol) FBS at 37°C with 5% CO_2. A549 cells, HeLa cells, primary small airway epithelial cells, Jurkat E6.1 T-cells, and PBMCs were stimulated with IFN-γ (Sigma-Aldrich, catalog no. SRP3058) at either 10 or 100 ng/mL for 24 h. After 24 h, cells were washed in phosphate-buffered saline (PBS; Quality Biological) and cultured for 24 h in complete growth medium. After 24 h, cells were restimulated with IFN-γ at either 10 or 100 ng/mL for 24 h.

Plasmids

The following plasmids were used in this study: the full-length HIV-1 clade B molecular clone pNL4-3 and derivatives pNL4-3/KFS (env-minus) (20) and pNL4-3.Luc.R-E- (21) (National Institutes of Health AIDS Reagent Program [NIH ARP], catalog no. 3418); HIV-1 Env expression vector pIIINL4env (25); and the VSV-G expression vector pHCMV-G (39, 40). pSVAMLVenv was obtained from N. Landau and D. Littman through the NIH ARP; pcDNA3.1(-)-SARS-CoV S vector and pcDNA3.1(-)-SARS-CoV-2 S vector for SARS-CoV-2 S from the Wuhan strain were gifts from Thomas Gallagher (Loyola University) (41); pCG-HA-GBP5 was a kind gift from Frank Kirchhoff (Ulm University, Germany); pCAGGS-TMPRSS2 vector was a kind gift from Stefan Poehlmann (German Primate Center, Germany); pMX-hCD4 was a gift from Dan Littman (Addgene plasmid #14614, http://n2t.net/addgene:14614, RRID: Addgene_14614); and pCMV-HA was obtained from Clontech (https://www.addgene.org/vector-database/2222/). The GBP5 C583A mutant was generated by PCR mutagenesis using PfuTurbo DNA polymerase (Agilent) using the following primers: GBP5 C583A_F (5′-GAGGACTGTTAATAACGATGATCCAGCCGTTTTA CTCTAA-3′) and GBP5 C583A_R (5′-TTAGAGTAAAACGGCTGGATCATCGTTATTAACAG-3′). Plasmids were purified using MaxiPrep kits (Qiagen, catalog no. 12163), and mutations were verified by DNA sequencing (Psomagen, Rockville, MD).

Preparation of virus stocks

HEK293T cells were transfected with the indicated plasmids using Lipofectamine 2000 (Invitrogen) according to the manufacturer's instructions. Virus-containing supernatants were filtered through a 0.45-µm membrane 48 h post-transfection; a portion was used in infectivity assays, and the remainder was used to collect virus particles by ultracentrifugation. Virus pellets and cells were solubilized in lysis buffer (10 mM iodoacetamide (Sigma-Aldrich), complete protease inhibitor tablets (Roche), 300 mM sodium chloride, 50 mM Tris-HCl (pH 7.5), and 0.5% (vol/vol) Triton X-100 (Sigma-Aldrich)] and used for further analysis. The amount of virus in the supernatant was quantified by the RT assay. RT assays were performed as described previously (42). Briefly, after incubation of the virus supernatants with RT reaction mixtures, which contained a template primer of poly(rA) (5 µg/mL) and oligo(dT)12–18 primers (1.57 µg/ mL), in 50 mM Tris (pH 7.8), 75 mM KCl, 2 mM dithiothreitol, 5 mM $MgCl_2$, 0.05% NP-40, and 0.25 µCi of ^{32}P-dTTP (3′-deoxythymidine 5′-triphosphate) at 37°C for 3 h, the mixtures were spotted onto positively charged nylon membrane (MilliporeSigma). After washing the nylon membranes with 2× SSC buffer (300 mM NaCl and 30 mM sodium citrate), levels of bound ^{32}P were measured on a Wallac MicroBeta2 microplate counter (PerkinElmer).

Western blotting

Cell and virus lysates were treated with 6× SDS-PAGE sample loading buffer (600 mM Tris-HCl [pH 6.8], 30%]vol/vol] glycerol, 12%]wt/vol] SDS, 20 mM dithiothreitol, and 0.03% [wt/vol] bromophenol blue) and heated at 95°C for 5 min. Samples were analyzed on either 7.5%, 12%, or 8%–16% Tris-glycine gels using a Bio-Rad Trans-Blot Turbo Transfer system according to the manufacturer's instructions. Proteins were detected with primary and secondary antibodies. Protein bands were visualized using chemiluminescence with a Sapphire Biomolecular Imager (Azure Biosystems) and analyzed with ImageJ 1.53k software. The following antibodies were used in this study: anti-HIV-1 Ig, anti-HIV-1 gp120 (16H3, catalog no. 12559), and anti-HIV-1 gp41 (clone Chessie 8, catalog no. ARP-13049) (obtained from the NIH ARP); anti-SARS-CoV/SARS-CoV-2 S (GeneTex, catalog no. GTX632604); anti-VSV-G (Cell Signaling, catalog no. 93372); anti-GBP5 (Cell Signaling, catalog no. 67798); anti-STAT-1 (Cell Signaling, catalog no. 14994); anti-alpha-tubulin (Sigma-Aldrich, clone B-5-1-2, catalog no. T5168); anti-CD4 (Santa Cruz, catalog no. sc-19641); goat anti-mouse IgG conjugated to horseradish peroxidase (HRP) (Invitrogen, catalog no. 31446); goat anti-rabbit IgG conjugated to HRP (Invitrogen, catalog no. 65-6120); and anti-human IgG conjugated to HRP (Sigma-Aldrich, catalog no. GENA933). Anti-A-MLV p15(E) Env antiserum was custom made in rabbits by Thermo Fisher Scientific using the peptide sequence C-RDSMALRERLNQRQKLFE (43). Rabbit anti-MLV-gp70 (DJ-39462) antibody specific for MoMuLV was kindly provided by R. J. Gorelick (AIDS and Cancer Virus, SAIC-Frederick).

Single-cycle infectivity assays

TZM-bl cells, a HeLa-derived cell line that contains a stably integrated HIV-LTR-luciferase cassette (23), were infected with serial dilutions of RT-normalized virus stock (42). For infectivity assays using SARS-CoV S and SARS-CoV-2 S-pseudotyped particles, HEK293T cells stably expressing hACE2 (BEI Resources, catalog no. NR-52511) transfected with TMPRSS2 expression plasmid were infected with serial dilutions of RT-normalized S-pseudotyped, luciferase-expressing HIV-1 (pNL4-3.Luc.R-E-) virus stock. Cells were lysed with BriteLite luciferase reagent (PerkinElmer), and luciferase activity was measured in a Wallac BetaMax plate reader at 48 h post-infection. Data were normalized to data for non-GBP5-transfected negative control from three independent experiments.

Flow cytometry

HEK293T cells (500,000) were resuspended in 500 µL PBS. To detect cell-surface glycoprotein, an antibody solution for target glycoprotein was made at a 1:1,000 dilution in PBS containing 1% (wt/vol) bovine serum albumin (BSA) (Bio-World, catalog no. 22070004–3). The following antibodies were used: anti-HIV-1 gp120 (IgG1 b12, obtained from Dr. Dennis Burton and Dr. Carlos Barbas through BEI Resources, catalog no. ARP-2640) to detect HIV-1 Env and Alexa Fluor 647-conjugated SARS-CoV-2 spike S1 subunit antibody (R&D Systems, clone 1035226, catalog no. FAB105805R) to detect SARS-CoV S and SARS-CoV-2 S. Cells were incubated with antibodies for 1 h at 4°C and then washed three times with PBS containing 1% (wt/vol) BSA. Goat anti-human antibody conjugated to Alexa Fluor 647 was used as a secondary antibody (Invitrogen, catalog no. A21445) at 1:1,000 in PBS containing 1% (wt/vol) BSA for cells expressing HIV-1 Env. Unbound antibody was removed with three PBS washes. Cells were then resuspended in 100-µL fixation/permeabilization solution (BD Biosciences, catalog no. 554714) and incubated for 30 min at room temperature. After fixation/permeabilization, cells were washed in 1× Perm/Wash buffer (BD Biosciences, catalog no. 554714) and incubated with an antibody cocktail containing PE-conjugated anti-HA.11 epitope tag antibody (Sony, clone 16B12, catalog no. 5107585) at a 1:1,000 dilution in 1× Perm/Wash buffer. Cells were incubated at 4°C for 1 h. Unbound antibody was removed with three 1× Perm/Wash buffer washes. Finally, cells were resuspended in 200-µL PBS and analyzed via a BD LSRFortessa flow cytometer (BD Bioscience). Data were exported as FCS3.0

files and analyzed with FlowJo version 10.9.0 software (Tree Star, Inc.). Briefly, cells were gated for HEK293T cells by light scatter followed by doublet discrimination in both side and forward scatters. A consistent gate was used to quantify the fraction of cells that expressed APC (glycoprotein).

Statistics

Statistics were calculated using GraphPad Prism version 10.2.0 for Mac OS (GraphPad Software, La Jolla, CA). Unpaired Student's *t*-tests were performed, and two-tailed *P* values of <0.05 were considered statistically significant. GraphPad Prism was also used to calculate standard deviations; data are shown as mean ± SD.

ACKNOWLEDGMENTS

We thank Thomas Gallagher (Loyola University), Frank Kirchhoff (Ulm University), and Alex Compton (NCI-Frederick) for providing plasmids for the study. We thank Yuta Hikichi for isolating and activating peripheral blood mononuclear cells, Sherimay Ablan and Geraldine V. Vilmen for technical advice, and all members of the Freed lab for critical review of the manuscript and helpful discussion. We thank Olga A. Nikolaitchik (NCI-Frederick) and David J. Turner (NCI-Frederick) for technical advice on flow cytometry.

Research in the Freed lab is supported by the Intramural Research Program of the Center for Cancer Research, National Cancer Institute, National Institutes of Health. Funds were also provided by a grant from an Intramural AIDS Research Fellowship (for H.V.).

H.V. and E.O.F. designed the research. H.V., C.M.L., and A.A.W. performed the research and analyzed the data. H.V. and E.O.F. wrote the paper.

AUTHOR AFFILIATION

[1]Virus-Cell Interaction Section, HIV Dynamics and Replication Program, Center for Cancer Research, National Cancer Institute, Frederick, Maryland, USA

AUTHOR ORCIDs

Hana Veler http://orcid.org/0009-0007-8733-5258
Eric O. Freed http://orcid.org/0000-0003-3345-022X

FUNDING

Funder	Grant(s)	Author(s)
HHS | NIH | National Cancer Institute (NCI)	ZIA BC 011721	Hana Veler

AUTHOR CONTRIBUTIONS

Hana Veler, Conceptualization, Data curation, Formal analysis, Funding acquisition, Investigation, Validation, Visualization, Writing – original draft, Writing – review and editing | Cheng Man Lun, Data curation, Formal analysis | Abdul A. Waheed, Data curation, Formal analysis, Writing – review and editing | Eric O. Freed, Conceptualization, Funding acquisition, Project administration, Resources, Supervision, Writing – original draft, Writing – review and editing

DIRECT CONTRIBUTION

This article is a direct contribution from Eric O. Freed, a Fellow of the American Academy of Microbiology, who arranged for and secured reviews by Chen Liang, Lady Davis Institute for Medical Research, and Alon Herschhorn, University of Minnesota Medical School Twin Cities.

ETHICS APPROVAL

Peripheral blood mononuclear cells were obtained from anonymous, deidentified blood donors through the NCI-Frederick Research Donor Program.

ADDITIONAL FILES

The following material is available online.

Supplemental Material

Fig. S1 (mBio02086-24-s0001.eps). Correlation between reduced viral glycoprotein incorporation and impaired particle infectivity induced by GBP5 expression.
Fig. S2 (mBio02086-24-s0002.eps). Isoprenylation-deficient C583A GBP5 mutant does not inhibit HIV-1 infectivity or the infectivity of HIV-1 virions pseudotyped with SARS-CoV or SARS-CoV-2 S.
Fig. S3 (mBio02086-24-s0003.eps). GBP5 expression increases the electrophoretic mobility of cell-associated HIV-1 Env, SARS-CoV-2 S, and SARS-CoV S.
Fig. S4 (mBio02086-24-s0004.eps). Overexpression of HIV-1 Env and SARS-CoV-2 S confers GBP5 resistance.
Fig. S5 (mBio02086-24-s0005.eps). GBP5 expression increases the electrophoretic mobility of CD4.
Legends (mBio02086-24-s0006.docx). Supplemental figure legends.

REFERENCES

1. Rey FA, Lok SM. 2018. Common features of enveloped viruses and implications for immunogen design for next-generation vaccines. Cell 172:1319–1334. https://doi.org/10.1016/j.cell.2018.02.054
2. Frabutt DA, Zheng YH. 2016. Arms race between enveloped viruses and the host ERAD machinery. Viruses 8:255. https://doi.org/10.3390/v8090255
3. Kielian M, Rey FA. 2006. Virus membrane-fusion proteins: more than one way to make a hairpin. Nat Rev Microbiol 4:67–76. https://doi.org/10.1038/nrmicro1326
4. Checkley MA, Luttge BG, Freed EO. 2011. HIV-1 envelope glycoprotein biosynthesis, trafficking, and incorporation. J Mol Biol 410:582–608. https://doi.org/10.1016/j.jmb.2011.04.042
5. Riley NM, Hebert AS, Westphall MS, Coon JJ. 2019. Capturing site-specific heterogeneity with large-scale N-glycoproteome analysis. Nat Commun 10:1311. https://doi.org/10.1038/s41467-019-09222-w
6. Thomas G. 2002. Furin at the cutting edge: from protein traffic to embryogenesis and disease. Nat Rev Mol Cell Biol 3:753–766. https://doi.org/10.1038/nrm934
7. Beitari S, Wang Y, Liu SL, Liang C. 2019. HIV-1 envelope glycoprotein at the interface of host restriction and virus evasion. Viruses 11:311. https://doi.org/10.3390/v11040311
8. Martens S, Howard J. 2006. The interferon-inducible GTPases. Annu Rev Cell Dev Biol 22:559–589. https://doi.org/10.1146/annurev.cellbio.22.010305.104619
9. Kim BH, Shenoy AR, Kumar P, Bradfield CJ, MacMicking JD. 2012. IFN-inducible GTPases in host cell defense. Cell Host Microbe 12:432–444. https://doi.org/10.1016/j.chom.2012.09.007
10. Anderson SL, Carton JM, Lou J, Xing L, Rubin BY. 1999. Interferon-induced guanylate binding protein-1 (GBP-1) mediates an antiviral effect against vesicular stomatitis virus and encephalomyocarditis virus. Virology (Auckl) 256:8–14. https://doi.org/10.1006/viro.1999.9614
11. Pan W, Zuo X, Feng T, Shi X, Dai J. 2012. Guanylate-binding protein 1 participates in cellular antiviral response to dengue virus. Virol J 9:292. https://doi.org/10.1186/1743-422X-9-292
12. Itsui Y, Sakamoto N, Kurosaki M, Kanazawa N, Tanabe Y, Koyama T, Takeda Y, Nakagawa M, Kakinuma S, Sekine Y, Maekawa S, Enomoto N, Watanabe M. 2006. Expressional screening of interferon-stimulated genes for antiviral activity against hepatitis C virus replication. J Viral Hepat 13:690–700. https://doi.org/10.1111/j.1365-2893.2006.00732.x
13. Itsui Y, Sakamoto N, Kakinuma S, Nakagawa M, Sekine-Osajima Y, Tasaka-Fujita M, Nishimura-Sakurai Y, Suda G, Karakama Y, Mishima K, Yamamoto M, Watanabe T, Ueyama M, Funaoka Y, Azuma S, Watanabe M. 2009. Antiviral effects of the interferon-induced protein guanylate binding protein 1 and its interaction with the hepatitis C virus NS5B protein. Hepatology 50:1727–1737. https://doi.org/10.1002/hep.23195
14. Feng J, Cao Z, Wang L, Wan Y, Peng N, Wang Q, Chen X, Zhou Y, Zhu Y. 2017. Inducible GBP5 mediates the antiviral response via interferon-related pathways during influenza A virus infection. J Innate Immun 9:419–435. https://doi.org/10.1159/000460294
15. Rhein BA, Powers LS, Rogers K, Anantpadma M, Singh BK, Sakurai Y, Bair T, Miller-Hunt C, Sinn P, Davey RA, Monick MM, Maury W. 2015. Interferon-γ inhibits Ebola virus infection. PLoS Pathog 11:e1005263. https://doi.org/10.1371/journal.ppat.1005263
16. McLaren PJ, Gawanbacht A, Pyndiah N, Krapp C, Hotter D, Kluge SF, Götz N, Heilmann J, Mack K, Sauter D, Thompson D, Perreaud J, Rausell A, Munoz M, Ciuffi A, Kirchhoff F, Telenti A. 2015. Identification of potential HIV restriction factors by combining evolutionary genomic signatures with functional analyses. Retrovirology Auckl 12:41. https://doi.org/10.1186/s12977-015-0165-5
17. Krapp C, Hotter D, Gawanbacht A, McLaren PJ, Kluge SF, Stürzel CM, Mack K, Reith E, Engelhart S, Ciuffi A, Hornung V, Sauter D, Telenti A, Kirchhoff F. 2016. Guanylate binding protein (GBP) 5 is an interferon-inducible inhibitor of HIV-1 infectivity. Cell Host Microbe 19:504–514. https://doi.org/10.1016/j.chom.2016.02.019
18. Braun E, Hotter D, Koepke L, Zech F, Groß R, Sparrer KMJ, Müller JA, Pfaller CK, Heusinger E, Wombacher R, Sutter K, Dittmer U, Winkler M, Simmons G, Jakobsen MR, Conzelmann KK, Pöhlmann S, Münch J, Fackler OT, Kirchhoff F, Sauter D. 2019. Guanylate-binding proteins 2 and 5 exert broad antiviral activity by inhibiting furin-mediated processing of viral envelope proteins. Cell Rep 27:2092–2104. https://doi.org/10.1016/j.celrep.2019.04.063
19. Mesner D, Reuschl AK, Whelan MVX, Bronzovich T, Haider T, Thorne LG, Ragazzini R, Bonfanti P, Towers GJ, Jolly C. 2023. SARS-CoV-2 evolution influences GBP and IFITM sensitivity. Proc Natl Acad Sci U S A 120:e2212577120. https://doi.org/10.1073/pnas.2212577120
20. Freed EO, Delwart EL, Buchschacher GL, Panganiban AT. 1992. A mutation in the human immunodeficiency virus type 1 transmembrane glycoprotein gp41 dominantly interferes with fusion and infectivity. Proc Natl Acad Sci U S A 89:70–74. https://doi.org/10.1073/pnas.89.1.70

21. Connor RI, Chen BK, Choe S, Landau NR. 1995. Vpr is required for efficient replication of human immunodeficiency virus type-1 in mononuclear phagocytes. Virology (Auckl) 206:935–944. https://doi.org/10.1006/viro.1995.1016
22. Adachi A, Gendelman HE, Koenig S, Folks T, Willey R, Rabson A, Martin MA. 1986. Production of acquired immunodeficiency syndrome-associated retrovirus in human and nonhuman cells transfected with an infectious molecular clone. J Virol 59:284–291. https://doi.org/10.1128/jvi.59.2.284-291.1986
23. Platt EJ, Wehrly K, Kuhmann SE, Chesebro B, Kabat D. 1998. Effects of CCR5 and CD4 cell surface concentrations on infections by macrophage-tropic isolates of human immunodeficiency virus type 1. J Virol 72:2855–2864. https://doi.org/10.1128/JVI.72.4.2855-2864.1998
24. Cui W, Braun E, Wang W, Tang J, Zheng Y, Slater B, Li N, Chen C, Liu Q, Wang B, Li X, Duan Y, Xiao Y, Ti R, Hotter D, Ji X, Zhang L, Cui J, Xiong Y, Sauter D, Wang Z, Kirchhoff F, Yang H. 2021. Structural basis for GTP-induced dimerization and antiviral function of guanylate-binding proteins. Proc Natl Acad Sci U S A 118:e2022269118. https://doi.org/10.1073/pnas.2022269118
25. Murakami T, Freed EO. 2000. The long cytoplasmic tail of gp41 is required in a cell type-dependent manner for HIV-1 envelope glycoprotein incorporation into virions. Proc Natl Acad Sci U S A 97:343–348. https://doi.org/10.1073/pnas.97.1.343
26. Simmons G, Gosalia DN, Rennekamp AJ, Reeves JD, Diamond SL, Bates P. 2005. Inhibitors of cathepsin L prevent severe acute respiratory syndrome coronavirus entry. Proc Natl Acad Sci U S A 102:11876–11881. https://doi.org/10.1073/pnas.0505577102
27. Ho DD, Rota TR, Hirsch MS. 1986. Infection of monocyte/macrophages by human T lymphotropic virus type III. J Clin Invest 77:1712–1715. https://doi.org/10.1172/JCI112491
28. Gartner S, Markovits P, Markovitz DM, Kaplan MH, Gallo RC, Popovic M. 1986. The role of mononuclear phagocytes in HTLV-III/LAV infection. Science 233:215–219. https://doi.org/10.1126/science.3014648
29. Baum C, Ostertag W. 1998. Lineage-tropism of murine leukemia virus enhancer activity within the hematopoietic system. In Hiddemann W (ed), Acute leukemias VII. Haematology and blood transfusion / hämatologie und bluttransfusion. Vol. 39. Springer, Berlin, Heidelberg. https://doi.org/10.1007/978-3-642-71960-8_52.
30. Lamers MM, Haagmans BL. 2022. SARS-CoV-2 pathogenesis. Nat Rev Microbiol 20:270–284. https://doi.org/10.1038/s41579-022-00713-0
31. Lyles D, Kuzmin I, Rupprecht C. 2013. Rhabdoviridae: the viruses and their replication, p 885–919. In Knipe D, Howley P (ed), Fields virology, 6th ed. Lippincott Williams & Wilkins, Philadelphia.
32. Ghosh S, Dellibovi-Ragheb TA, Kerviel A, Pak E, Qiu Q, Fisher M, Takvorian PM, Bleck C, Hsu VW, Fehr AR, Perlman S, Achar SR, Straus MR, Whittaker GR, de Haan CAM, Kehrl J, Altan-Bonnet G, Altan-Bonnet N. 2020. β-coronaviruses use lysosomes for egress instead of the biosynthetic secretory pathway. Cell 183:1520–1535. https://doi.org/10.1016/j.cell.2020.10.039
33. Sa Ribero M, Jouvenet N, Dreux M, Nisole S. 2020. Interplay between SARS-CoV-2 and the type I interferon response. PLoS Pathog 16:e1008737. https://doi.org/10.1371/journal.ppat.1008737
34. Acosta PL, Byrne AB, Hijano DR, Talarico LB. 2020. Human type I interferon antiviral effects in respiratory and reemerging viral infections. J Immunol Res 2020:1372494. https://doi.org/10.1155/2020/1372494
35. Zhang Q, Bastard P, Liu Z, Le Pen J, Moncada-Velez M, Chen J, Ogishi M, Sabli IKD, Hodeib S, Korol C, et al. 2020. Inborn errors of type I IFN immunity in patients with life-threatening COVID-19. Science 370:eabd4570. https://doi.org/10.1126/science.abd4570
36. Zhong L, Song Y, Marziali F, Uzbekov R, Nguyen XN, Journo C, Roingeard P, Cimarelli A. 2022. A novel domain within the CIL regulates egress of IFITM3 from the Golgi and reveals a regulatory role of IFITM3 on the secretory pathway. Life Sci Alliance 5:e202101174. https://doi.org/10.26508/lsa.202101174
37. Kukuruzinska MA, Bergh MLE, Jackson BJ. 1987. Protein glycosylation in yeast. Annu Rev Biochem 56:915–944. https://doi.org/10.1146/annurev.bi.56.070187.004411
38. Wang S, Li W, Wang L, Tiwari SK, Bray W, Wu L, Li N, Hui H, Clark AE, Zhang Q, Zhang L, Carlin AF, Rana TM. 2024. Interferon-inducible guanylate-binding protein 5 inhibits replication of multiple viruses by binding to the oligosaccharyltransferase complex and inhibiting glycoprotein maturation. bioRxiv:2024.05.01.591800. https://doi.org/10.1101/2024.05.01.591800
39. Burns JC, Friedmann T, Driever W, Burrascano M, Yee JK. 1993. Vesicular stomatitis virus G glycoprotein pseudotyped retroviral vectors: concentration to very high titer and efficient gene transfer into mammalian and nonmammalian cells. Proc Natl Acad Sci U S A 90:8033–8037. https://doi.org/10.1073/pnas.90.17.8033
40. Yee JK, Miyanohara A, LaPorte P, Bouic K, Burns JC, Friedmann T. 1994. A general method for the generation of high-titer, pantropic retroviral vectors: highly efficient infection of primary hepatocytes. Proc Natl Acad Sci U S A 91:9564–9568. https://doi.org/10.1073/pnas.91.20.9564
41. Qing E, Gallagher T. 2023. Adaptive variations in SARS-CoV-2 spike proteins: effects on distinct virus-cell entry stages. mBio 14:e0017123. https://doi.org/10.1128/mbio.00171-23
42. Willey RL, Smith DH, Lasky LA, Theodore TS, Earl PL, Moss B, Capon DJ, Martin MA. 1988. *In vitro* mutagenesis identifies a region within the envelope gene of the human immunodeficiency virus that is critical for infectivity. J Virol 62:139–147. https://doi.org/10.1128/JVI.62.1.139-147.1988
43. Waheed AA, Zhu Y, Agostino E, Naing L, Hikichi Y, Soheilian F, Yoo SW, Song Y, Zhang P, Slusher BS, Haughey NJ, Freed EO. 2023. Neutral sphingomyelinase 2 is required for HIV-1 maturation. Proc Natl Acad Sci U S A 120:e2219475120. https://doi.org/10.1073/pnas.2219475120